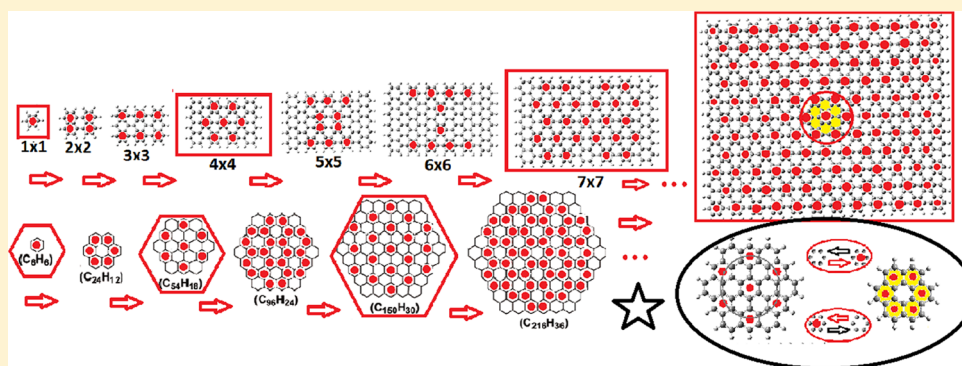


A Pedestrian Approach to the Aromaticity of Graphene and Nanographene: Significance of Huckel's $(4n+2)\pi$ Electron Rule

Aristides D. Zdetsis^{*,†,‡} and E. N. Economou[‡][†]Molecular Engineering Laboratory, Department of Physics, University of Patras, Patras 26500 GR, Greece[‡]Institute of Electronic Structure and Laser, Foundation for Research & Technology Hellas, Vassilika Vouton, P.O. Box 1385, Heraklion, Crete GR 71110, Greece

ABSTRACT: In an attempt to describe and rationalize the elusive aromatic properties of graphene by first-principles calculations in a simple and transparent way, we have constructed numerous judiciously chosen real-space models of various sizes and symmetries, which lead to the aromaticity pattern of infinite graphene by a process of “spatial” evolution through successive peripheral additions, characterized by fundamental periodicities related to the traditional Huckel $(4n+2)\pi$ electron rule. In accord with the early expectations of Pauling, we have found that the electronic and aromatic properties of infinite graphene result from the superposition of two complementary primary aromatic configurations, in which full and empty rings are interchanged. The primary pattern consists of a hexagonal superlattice in which each fully aromatic ring is surrounded by six nonaromatic rings, in full agreement with the empirical Clar aromatic sextet theory. We have found that, for finite nanographene(s), aromaticity patterns change periodically by addition/removal of one periphery of rings, which for hexagonal samples is equivalent to exchanging aromatic and nonaromatic rings, resulting in alternating $(4n+2)$ and $4n$ π electron numbers, characterizing, respectively, “aromatic” and “anti-aromatic” samples according to Huckel’s $(4n+2)\pi$ electron rule. For infinite graphene, this interchange occurs naturally, resulting in a uniform pattern. The opposite route is also valid, subject to the restrictions of size and edge morphology, which determine and “tune” the aromaticity pattern(s). The observed periodicities in the aromaticity patterns of graphene nanoribbons and carbon nanotubes are rooted in such fundamental “peripheral” periodicities. These findings, on top of their fundamental importance, should be very useful for the technological functionalization of infinite and finite graphene and graphene-based materials.

1. INTRODUCTION

The electronic properties of graphene are characterized primarily by the network of mobile (delocalized) π electrons based on the atomic p_z orbitals, while the σ bonding is assumed to be a rigid honeycomb framework built out of “localized” (sp^2 hybridized) two-center two-electron ($2c-2e$) C–C σ bonds. Delocalized π bonding is naturally described by the concept of aromaticity,^{1,2} which, however, is not free of controversial and conflicting views open to debate, even today.^{1–3} Aromaticity, initially described by the traditional Huckel $(4n+2)\pi$ electron rule (which is strictly applied to monocyclic systems as benzene), is not a measurable quantity and is usually described by various “aromaticity indices” (or aromaticity criteria), based on bonding, electronic, magnetic, etc., characteristics, which, however, are neither unique nor fully compatible among

themselves.^{1–3} In general, aromaticity involves planarity and extra stability due to electron delocalization, like benzene. In fact, the qualitative meaning of aromaticity is “like benzene”. Therefore, since benzene is considered as the prototypical aromatic molecule, then graphite, and par excellence graphene, should be thought of as more aromatic than benzene, since the resonance energy per π electron of graphite is greater than that in benzene.⁴ Then, the answer to the question “is graphene aromatic?”⁵ should, apparently, be affirmative but not as trivial as in the case of benzene. In graphene, the number of π electrons which could be assigned to a particular ring is two

Received: May 5, 2015

Revised: June 25, 2015

instead of six, since each of the six carbon atoms of this ring belongs to three adjacent rings and, therefore, contributes only one-third of its two π electrons. On the basis of this, Popov et al.⁵ considered highly electron-depleted small fragments such as $C_6H_6^{4+}$, $C_{24}H_{12}^{10+}$, and $C_{54}H_{18}^{16+}$ which have two electrons per ring (total numbers of electrons 2, 14, and 38, respectively) and studied their aromatic properties. On the basis of their findings, they concluded that graphene is aromatic but only locally with two π electrons localized over every ring. Nevertheless, the feature of carbons belonging to more than one ring is common to many organic aromatic molecules such as coronene or circumcoronene and other polycyclic benzenoid hydrocarbons (PBHs). Depending on the annelation modes of rings in PBHs, there are nine different values, ranging from 2 to 5, that the atom-based π electron ring content can obtain.⁶ Alternatively, one can use bond-based π electron distribution in rings (according to the local environment), which is more sensitive to cyclic electron conjugation (see Gutman et al.⁶). Thus, depending on the π electron distribution, some rings could be more aromatic than others or not aromatic at all. This is described by the “aromaticity pattern” of the particular polycyclic aromatic hydrocarbon (PAH), which is rationalized on the basis of “Clar’s aromatic sextet theory”.^{6–8} This theory, which is not free of limitations,⁷ assigns the proper Clar structure on the basis of “Clar’s rule”. Clar’s rule states that the Kekulé resonance structure with the largest number of disjoint aromatic π sextets, which is called the “Clar formula”, is the most important for characterization of the properties of PAHs. Aromatic π sextets are defined as six π electrons localized in a single benzene-like ring separated from adjacent rings by formal CC single bonds.^{6–8} According to Clar’s scheme, PAHs can be classified to those that have only π sextets and “empty” rings called by Clar “fully benzenoid”, those that have π sextets and rings with a single double bond, and those that have rings with two double bonds for which one can write more than a single Clar structure, as in coronene (migrating sextets).

In the present investigation, since aromaticity is primarily a molecular property, we are approaching the aromaticity of graphene through real space molecular models or “nanographenes” (NGRs) and PAHs, of various shapes and sizes from about 10 to 60 Å (containing up to 4900 electrons), which are treated through accurate *ab initio* real space all-electron density functional theory (DFT) and good quality basis sets. This real space approach, judiciously extrapolated, yields a unique aromaticity pattern of graphene, which consists of a periodic array (superlattice) of circumcoronene (CIRCO) or hexabenzocoronene (HEXCO) patterns. This is fully compatible with Clar’s sextet theory, as well as other intuitive results for finite (or semifinite) graphene systems, such as GNRs^{10–13} and nanotubes.¹³ The present approach has the added advantage of facilitating the transparent study and correlation of the various aromaticity patterns in terms of size, geometry, symmetry and topology, growth pattern, as well as changes in the boundaries or the perimeters of the “samples”. Furthermore, it can deal with special cases where the electron delocalization shows characteristics well beyond the common concepts of local and global aromaticity. This last characteristic is very important for graphene, in which bonding is shown to be an intrinsically collective phenomenon,¹⁴ in full accord with the results obtained here, and the expectations of Pauling.¹⁵ Following this approach, we have found (and rationalize) a remarkable periodicity in the aromaticity patterns of nanographene(s) as we add or remove one full layer of rings around

(or in one side of) the sample(s), which is analogous to the periodicity of the aromaticity patterns found in both GNRs^{10–13} and nanotubes,¹³ in terms of size (width/length). This periodicity is similar (equivalent) to the periodic changes in the aromaticity of homocentric hexagonal PAHs in terms of size as we go from benzene to coronene (CO) and then to circumcoronene (or hexabenzocoronene), etc. (see, for instance, Figure 11 below). Every time a new hexagonal periphery is added, the CIRCO (or HEXCO) and CO patterns are successively interchanged (Figure 11). In the limit of infinite graphene, as is further explained below, the two results (from the N th and $N+1$ th “peripheries”) should be superimposed, resulting in a uniform pattern which is consistent with the uniform lattice constant of graphene and the results of other theoretical works on the aromaticity of graphene, such as Popov et al.⁵ However, our results have far reaching consequences, going far beyond the results of Popov et al. in the sense of being more transparent and explicit, showing the resonance structure of graphene and the “dynamically uniform” aromaticity pattern, in accord with the results of Zubarev et al.¹⁴ In addition, our results can fully account for all observed periodicities of finite and semifinite graphene samples.^{10–13} Since the electronic properties are directly related to the aromaticity patterns,^{10–13} all of these “regularities”, routed to the “circumference periodicity” which will be further rationalized below, should be very important for future functionalization of graphene and nanographene(s). The structure of the paper is organized as follows: After the introduction in section 1, we present a “methods” section (section 2) describing briefly the theoretical and computational methods and techniques used in the present work. The methods section is followed by section 3 which presents our results together with their interpretation and discussion. Section 3 is logically divided into three subsections 3.1–3.3. In subsection 3.1, the limit of graphene is approached through various properly selected NGR models of representative sizes and geometries (including edge structure) of mainly D_{2h} and D_{6h} symmetries. The latter includes some selected particular PAHs seen practically as graphene models and not real molecules. Subsection 3.2 presents the opposite route from subsection 3.1, dealing with the periodicities and regularities in the aromaticity patterns of finite graphene samples, such as NGRs, nanoribbons, and nanotubes, related to the periodic aromaticity of graphene. Finally, in subsection 3.3, the same limit of infinite graphene is approached by a growing sequence of real PAHs with larger and larger diameters with alternating CO and HEXCO (or CIRCO) Clar type of aromaticity patterns. This has the added advantage of bringing up hidden symmetries and regularities which elucidate key aromatic and bonding characteristics of graphene, revealing at the same time the interrelation of the two approaches and the role of symmetry. The main conclusions of this work are summarized in the final section 4.

2. METHODOLOGY

2.1. Some Technical Details. To construct the aromaticity patterns of our models and assess their aromaticity, we have chosen to use one of the widely used, simple, transparent, and readily available aromaticity indices based on magnetic characteristics, expressed through the nucleus independent chemical shifts (NICS). Obviously, bonding criteria of aromaticity are not appropriate here, since we are, eventually, interested in infinite graphene of well-known bond length. The NICS criterion was introduced by Schleyer and co-workers⁹

(see also articles in refs 1 and 2). It is defined as the negative value of the absolute shielding computed at a ring center, NICS(0), or at some other point, usually at 1 Å above the ring center, NICS(1). Rings with large negative NICS values are considered aromatic, whereas rings with positive NICS values are regarded as anti-aromatic. NICS, and in particular NICS(1), without being free of criticism, has several advantages among other indicators of aromaticity: It is very accessible and easy to compute; it can be used to discuss both the local and the global aromaticity of molecules; and, finally, it does not use reference values, so it can be easily applied to any molecule⁴ or “supermolecule”. Obvious improvements of the NICS concept,^{1–3} such as the use of NICS (0 or 1) tensor components¹⁶ NICS(0)_{zz} and NICS(1)_{zz} or even better the π contribution to these components, NICS(0) _{π zz} and NICS(1) _{π zz} are not used in the present study, not only because they are clearly impractical (due to the large number and large size of the “molecules”) but they are also not needed for drawing our conclusions. For all DFT calculations (geometries, energies, NICS), we have used the Gaussian program package¹⁷ employing the hybrid PBE0¹⁸ functional and the 6-31G(d) basis set in this package. Thus, the level of our DFT results can be characterized as PBE0/6-31G(d), in the usual notation. Our models consist of (a) several hexagonal PAHs of D_{6h} symmetry, the smallest of which is coronene ($C_{24}H_{12}$) consisting of 36 atoms and the largest ($C_{252}H_{48}$) consisting of 300 atoms (1560 electrons), and (b) rectangular nanographene models of C_{2v} and D_{2h} symmetry with both armchair and zigzag edges passivated by hydrogen, of sizes (length/width) from 1 to 6 nm, up to 872 atoms (4832 electrons). All (hexagonal) PAHs, treated as real molecules, were fully optimized (under the D_{6h} symmetry constraint) at the DFT PBE0/6-31g(d) level, whereas for most of the D_{2h} -symmetric rectangular models the C–C bond distance was fixed at the graphene 1.42 Å value, since these mainly act as graphene models, not real molecules. As was verified by further optimization in many cases, geometry optimizations did not alter the overall aromaticity pattern, nor the relative NICS values (only some absolute values of the peripheral rings). This is a very important advantage of the NICS criterion, compared to other bond based criteria of aromaticity. The NICS(0) and NICS(1) were calculated at a large network of ring centers, using the gauge-independent-atomic-orbital (GIAO) method as implemented in the Gaussian package.¹⁷ Using the centers of each ring as “ghost atoms”, we have constructed a network of NICS(0) and NICS(1) values, the *NICS-maps*, indicating in a ball-and-stick diagram the “aromatic rings” (those with large negative values of NICS(1), larger or equal to the corresponding value of benzene, -11.4 ppm) at the present level of theory) with full red (on line) circles, in analogy to the red rings of Moran et al.⁴ (see Figure 1 in ref 4, and below). Much smaller (than -11.4 ppm) NICS values have been ignored. In several cases of “samples” with different ranges of aromatic NICS(1) values (larger than -11.4 ppm), we use variable size circles, proportional to the NICS(1) absolute values. As will be illustrated below, in the cases of pure Clar sextets, the NICS maps coincide with the Clar aromaticity patterns. In cases that we have rings with two double bonds for which one can write more than a single Clar structure, as in coronene, then, according to Clar, we have “migrating sextets”. In such a case, the NICS maps should be analogous to the superposition of the aromatic alternatives suggested by the “migration scheme”, indicated by arrows in Clar’s formula, as in ref 4 (see, for instance, Figures 1a and 3a).

3. RESULTS AND DISCUSSION

3.1. From Nanographenes to Graphene. *3.1.1. Hexagonal PAHs as Nanographene Models.* As the simplest nanographene (NGR) and graphene models, we can consider first some representative PAHs, the smallest of which (after benzene) is coronene. Coronene ($C_{24}H_{12}$), shown in Figure 1,

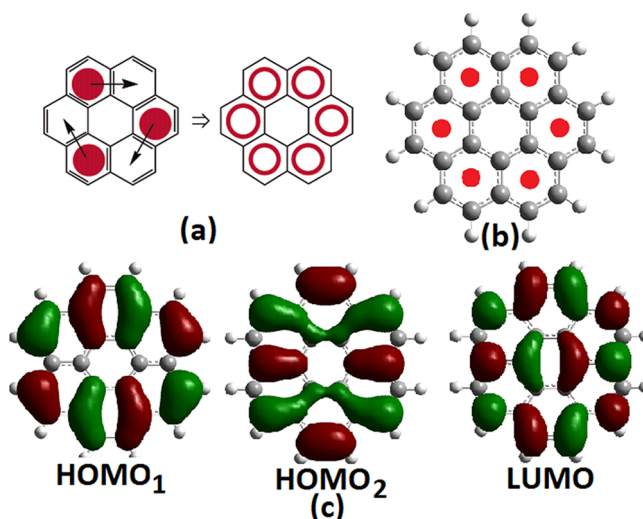


Figure 1. (a) Kekulé structure of coronene, with arrows indicating Clar sextet migration (left), together with their superposition leading to the NICS aromaticity pattern on the right (adopted from Moran et al.⁴). (b) Ball-and-stick NICS(1) aromaticity diagram and (c) calculated frontier orbitals of coronene (isovalue = 0.02).

which can be described as six (or seven) fused benzenoid rings, can be considered as a starting model in a sequence of models approaching that of graphene (or graphite). This will be considered in full detail in section 3.3. Coronene is believed to be superaromatic,⁴ although it does not satisfy Huckel’s $(4n + 2)\pi$ electron rule. The calculated NICS values at the rings’ centers suggest that the central ring is substantially less aromatic (NICS(1) = -5.4 ppm) than the fully aromatic peripheral rings (NICS(1) = -13.1 ppm). This is clearly indicated by the NICS map of Figure 1. In the same figure (Figure 1a, adopted from Moran et al.⁴), we can see the Kekulé structure of coronene and the corresponding Clar sextets in large solid circles. According to Clar, the aromaticity of coronene is enhanced by the migration of sextets according to the arrows, which creates an extra current. Such migration leads to a superposition pattern,⁴ indicated by the open circles in Figure 1a and by the solid circles in the NICS map of Figure 1b.

The aromaticity pattern would be expected to be related to the structure of the frontier orbitals, in particular the HOMOs. As indicated in Figure 1c, this is indeed the case. The structure of the frontier orbitals (usually HOMO and LUMO), which can be probed by scanning tunneling microscope (STM), also reflects the distribution of π electrons in PAHs, which, in turn, is well described by Clar’s formula.⁶ As a result, we can have remarkable similarities between aromaticity patterns described by Clar’s formula and STM images of PAHs,⁶ on the premise that rings which have a π sextet according to the Clar structure are more visible than those without the π sextet.⁸ This is clearly illustrated in Figure 2, in which the STM current image of hexabenzocoronene ($C_{42}H_{18}$) and the Clar formula, adopted from Gutman et al.,⁶ is shown together with the map obtained here (Figure 2b), and the calculated HOMO orbitals (Figure

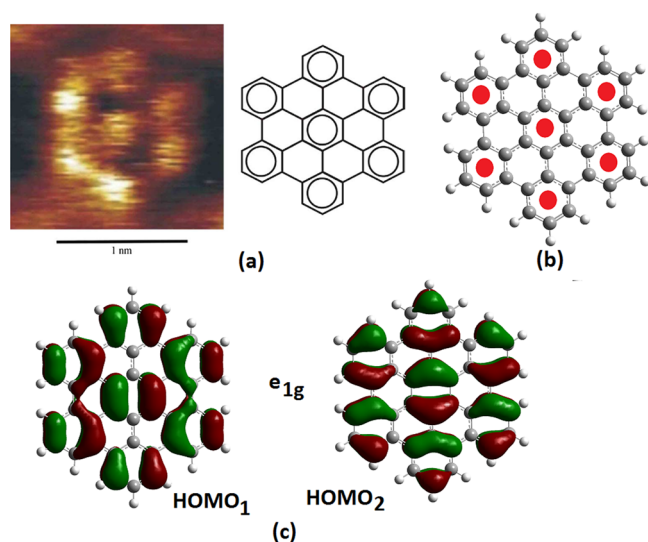


Figure 2. (a) STM current image of hexabenzocoronene ($C_{42}H_{18}$) and the corresponding Clar aromatic sextet formula (adopted from Gutman et al.⁶). (b) Ball-and-stick NICS(1) aromaticity diagram. (c) The two degenerate HOMO orbitals (isovalue = 0.02).

2c), which show remarkable similarity to both the STM image and the Clar formula, which in this case coincides with the calculated NICS map. Hexabenzocoronene (HEXCO) is fully consistent with Clar's theory (without invoking migrating sextets) corresponding to a Clar structure. The central ring in hexabenzocoronene is not only aromatic (reflected both in the structure of the frontier orbitals and the STM image), but it is more aromatic than the peripheral rings. The calculated NICS(1) value of the central ring is -15.3 ppm (NICS(0) = -13.6), whereas the peripheral rings are characterized by NICS(1) = -11.6 ppm, at the level of PBE0/6-31G(d).

A larger hexagonal PAH which is pretty much similar to coronene as far as the aromaticity pattern is involved (with a CO type of pattern involving migrating sextets) is $C_{96}H_{24}$ shown in Figure 3. The larger circles in the NICS map in Figure

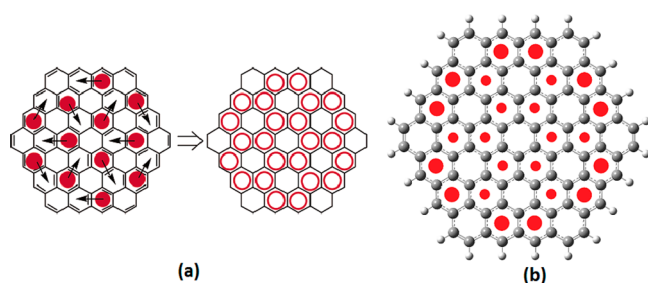


Figure 3. (a) Kekulé structure and Clar's formula of hexagonal $C_{96}H_{24}$ with arrows indicating the Clar sextet migration (left), together with the resulting NICS aromaticity pattern on the right (adopted from Moran et al.⁴). (b) Ball-and-stick NICS map calculated here.

3b correspond to NICS(1) = -17.1 ppm, and the smaller circles, to NICS(1) = -15.1 ppm. As we can see in Figure 3, the aromaticity pattern is a repeated (7 times) CO pattern, and as a consequence, the NICS topography is a superposition of the migrating sextets. In agreement with the results of Sakamoto et al.,¹⁹ obtained by a different method (the superaromatic stabilization energy), the aromaticity pattern in Figure 3 develops from the edges to the center. In other words,

the NICS(1) values at the edges are larger compared to the ones around the center.

However, according to our results, this is not always so, as we can see in Figure 4, showing the aromaticity pattern and the frontier orbitals of $C_{114}H_{30}$ which is another (Clar type) larger hexagonal PAH. $C_{114}H_{30}$ has a CIRCO aromaticity pattern (Clar formula), consisting of a hexagonal repeated motif, which “develops” and expands this time from the central region to the periphery (similarly to hexabenzocoronene where the NICS(1) value for the central ring is larger compared to the ones in the periphery). Here too the aromatic rings of the Clar type hexagonal pattern are characterized by larger NICS(1) absolute values (-16.4 ppm for the central ring and -15.3 ppm for the side rings) compared to the periphery, where the NICS(1) value reduces to -12.4 ppm. This is reflected in the size of the red circles indicating the aromatic or “nicsomatic” rings in the NICS map of Figure 4. Our results for this polybenzenoid PAH are in very good agreement with those of Moran et al.⁴ (see structure #5 in their Figure 3).

The frontier orbitals seem to be quite analogous to the aromaticity pattern, but sometimes, depending on the isovalue, this picture could be misleading, especially in comparisons with NICS maps, in which (for clarity's sake) aromatic rings with lower aromaticity have been omitted. This is emphatically illustrated in Figure 5, describing another larger ($C_{216}H_{36}$) non-Clar PAH with a CO type of pattern, in which the aromaticity (NICS) pattern of $C_{216}H_{36}$ is shown in two versions and the corresponding frontier orbitals are shown for two different isovalues (0.2 and 0.1). This large hexagonal PAH (which here serves as a NGR model) is characterized by three different regions of NICS(1), namely, -19 , -18 , and -16 ppm, indicated by circles of different size in the figure. In the first part of Figure 5 (Figure 5a), we retain only very aromatic rings with NICS(1) around -19 and -18 ppm. In this part of the figure, the frontier orbitals are drawn with the (more or less) standard isovalue of 0.2. In the second part of the figure (Figure 5b), all aromatic rings (with NICS(1) around -16 (or -15.5) ppm) are included and the corresponding isovalue for the frontier orbitals is lowered to 0.1. In both parts, we have good analogy of the aromaticity pattern and the frontier orbitals, but clearly, part b gives the complete picture, which illustrates multiple coronene motifs. It could also be interesting to draw the corresponding migration of Clar sextets, as in Figures 2 and 4. However, this would add unnecessary complication in the figures which is not essential for the purposes of this work. The interested reader could consult ref 17 for this purpose. This type of variation of the aromaticity pattern in terms of NICS(1) size allows the schematic illustration of the spatial “evolution” or “development” of the aromaticity pattern, from regions of higher aromaticity (in the periphery for CO type or central region for CIRCO/HEXCO type) to regions of lower (but still at least as high as benzene) aromaticity.

This is illustrated in Figure 6, which shows the “evolution” of the aromaticity pattern of $C_{252}H_{48}$ which is the largest hexagonal NGR model (PAH) considered here (Figure 6a), and $C_{114}H_{30}$ (Figure 6b). As can be seen in Figure 6a, one can distinguish four regions of aromatic NICS(1) values: one around -16 ppm (-16.07), another region around -15 ppm (from -14.97 to -14.53 ppm), -13 ppm (-12.98), and the final region around -12 ppm (-11.55 to -12.20 ppm), which completes the network of the CO type of hexagonal motifs. We can also see that the aromaticity pattern develops from regions around the surface, and in particular around the “crown” type of

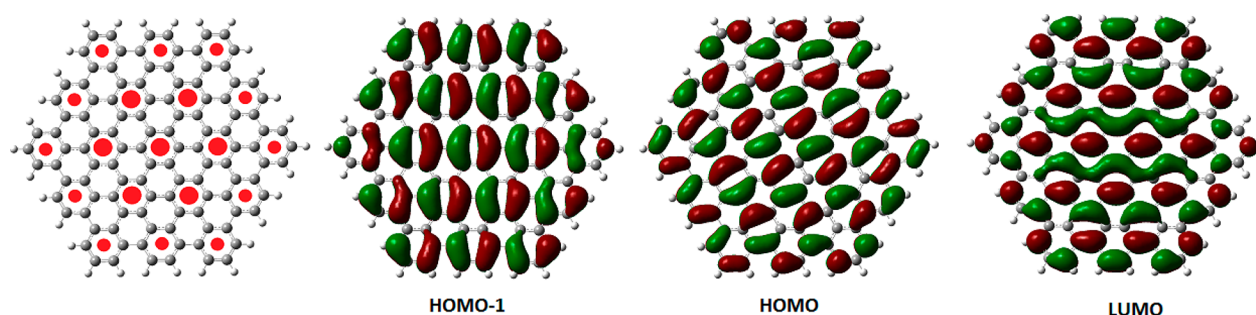


Figure 4. Aromaticity pattern of the hexagonal $C_{114}H_{30}$ NGR/PAH, together with the calculated frontier orbitals (isovalue = 0.01).

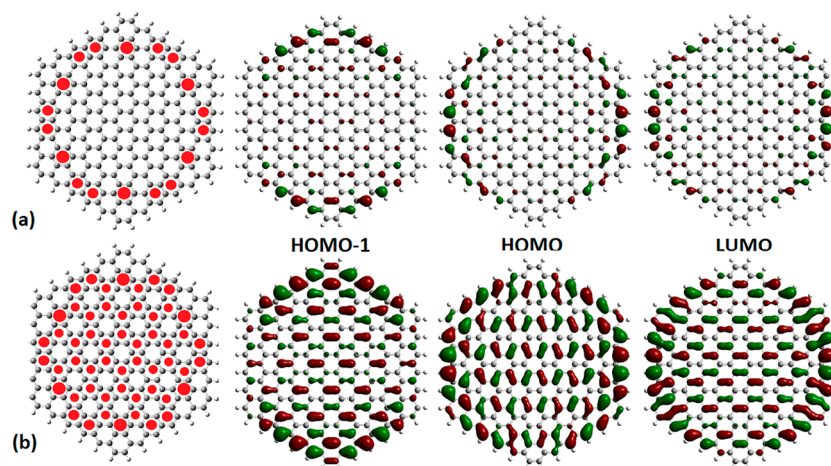


Figure 5. Aromaticity pattern of the large hexagonal $C_{216}H_{36}$ PAH, including only the largest magnitude (-19 and -18 ppm) NICS(1) values in part a and the rest (-16 ppm) in part b, together with the calculated frontier orbitals with isovalue = 0.02 (a) and isovalue = 0.01 (b).

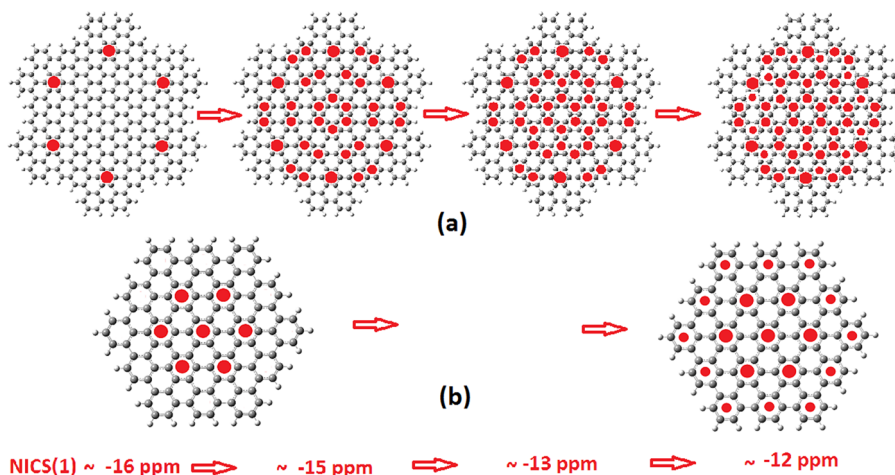


Figure 6. “Evolution” of the aromaticity pattern of $C_{252}H_{48}$ (a) and $C_{114}H_{30}$ (b) in terms of the range of aromatic NICS(1) values considered.

bonds (consisting of two successive armchair bond arrangements), toward the central region, similarly to $C_{216}H_{36}$, as can be seen in Figure 5. Parenthetically, it should be mentioned that the “crown” bonds, present also in hexabenzocoronene and $C_{114}H_{30}$, should be considered as very stable, or even aromatic.

However, as we have explained before, and as can be seen in Figure 6a, this type of spatial development of the aromaticity pattern (from surface to center) is not always the case in particular for Clar structures (CIRCO), contrary to what would be expected on the basis of Sakamoto’s¹⁹ conclusions. Clearly, the aromaticity pattern of $C_{114}H_{30}$, shown in Figures 4 and 6a, “develops” from the central ring toward the boundaries. This is

also true for hexabenzocoronene ($C_{42}H_{18}$) in which the central ring is more aromatic compared to the peripherals. Figures 5 and 6 also illustrate a well-known but often overlooked fact that the “empty” rings in the aromaticity patterns are not really empty but are characterized by (substantially) lower local π electron density compared to “full” rings, corresponding to “considerably” lower NICS values. More on this can be found in ref 17.

3.1.2. Generalizing to Rectangular and Hexagonal NGRs. So far, we have considered only hexagonal NGR models, which in reality are real PAHs, although rectangular NGRs are more common and familiar in graphene and nanographene studies.

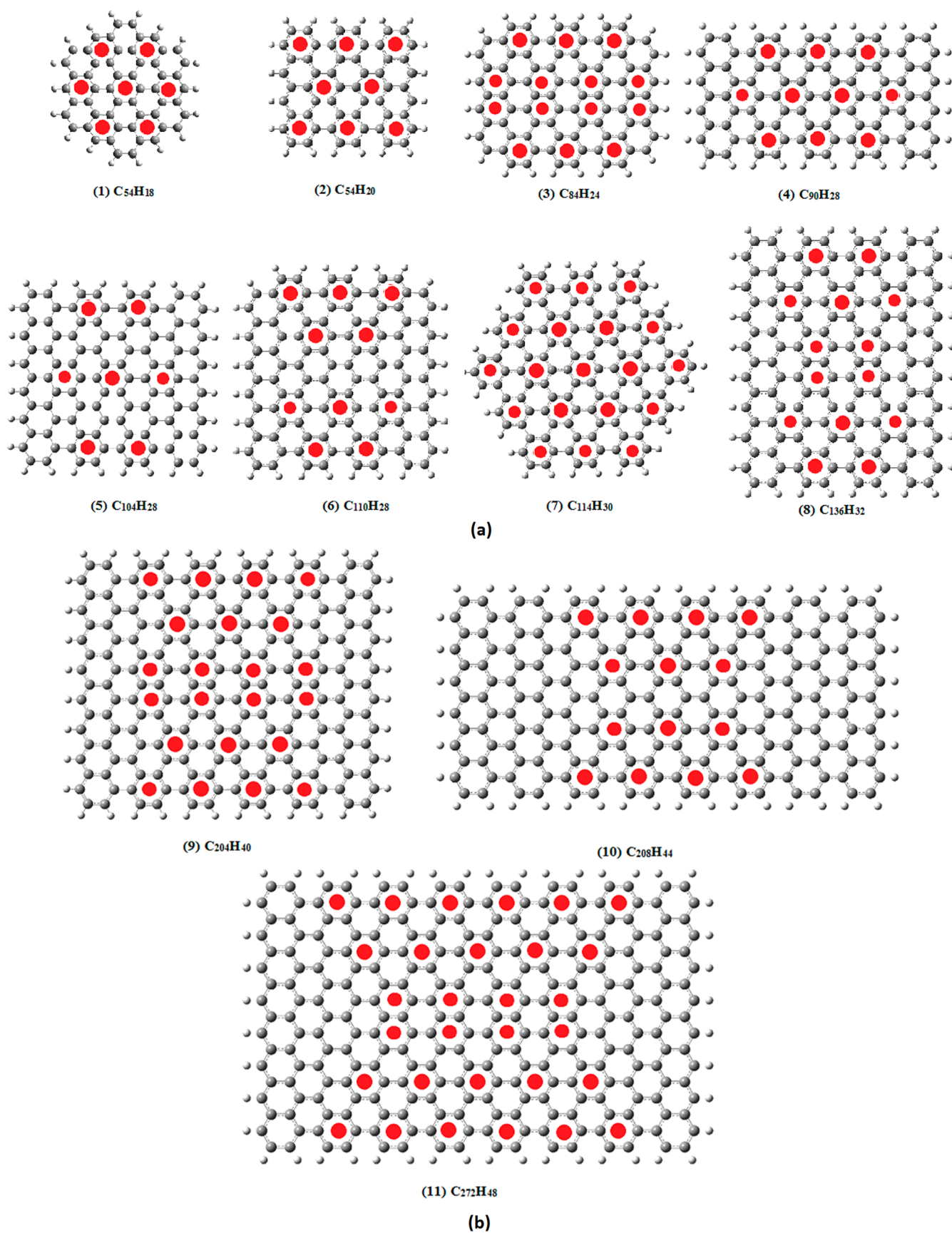


Figure 7. Aromaticity pattern of various rectangular and hexagonal NGRs of medium (a) and larger (b) sizes.

On the basis of the results obtained above for the hexagonal NGRs/PAHs, we have encountered two leading aromaticity

patterns CO and CIRCO (or Clar type). The CIRCO or Clar type is, loosely speaking, “less surface-dependent” in the sense

Table 1. Reference Number (#), Symmetry (symm.), and Composition (compos.) of the Structures in Figures 7 and 8, Together with Their Higher (NICS(1) H) and Lower (NICS(1) L) Values, Indicated with Larger and Smaller Circles in the Figure(s); the HOMO–LUMO Gap (H–L Gap); and Structural Characteristics (AxZ/struct.), Indicating (Wherever Is Applicable) the Number of Armchair (A) and Zigzag (Z) Rings in Their Periphery

#	symm.	compos.	NICS(1) H (ppm)	NICS(1) L (ppm)	H–L (eV)	AxZ/struct. (comments)
1	D_{6h}	$C_{54}H_{18}$	–17.5	–16.5	3.29	circumcoronene
2	D_{2h}	$C_{54}H_{20}$	–13.3	–11.2	0.27	3×4 half of (9)
3	D_{2h}	$C_{84}H_{24}$	–14.1	–11.8	2.72	$3(4) \times 4$, (2) + $1 \times 2A$
4	D_{2h}	$C_{90}H_{28}$	–13.5	–11.6	0.18	5×4 , (2) + $2 \times 2A$
5	D_{2h}	$C_{104}H_{28}$	–12.9	–11.2	0.23	4×6 , (9) – 2 peripheries
6	C_{2v}	$C_{110}H_{28}$	–13.9	–11.2	0.28	$3(4) \times 6$ (3) + 2 layers
7	D_{6h}	$C_{114}H_{30}$	–16.4	–12.3	2.60	D_{6h}
8	D_{2h}	$C_{136}H_{32}$	–13.0	–10.0 ^a	0.21	4×8
9	D_{2h}	$C_{204}H_{40}$	–14.6	–11.2	0.32	6×8 , $2 \times (2)$, (5) + periph.
10	D_{2h}	$C_{208}H_{44}$	–12.12	–11.3	0.11	8×6 “conjugate” (9)
11	D_{2h}	$C_{272}H_{48}$	–14.1	–12.3	0.25	8×8
12	D_{2h}	$C_{792}H_{80}$	–16.1	–11.2	0.17	12×16 (Figure 8)

^aNICS smaller than benzene but retained for clarity and completeness.

described above in Figures 5 and 6. This could have some real meaning when these PAHs are seen as models for approaching graphene, rather than real molecules, as we are doing here in this section. In this sense, the HEXCO aromaticity pattern (in Figures 2 and 4) could be very helpful and highly suggestive for assessing and classifying the NICS(1) aromaticity patterns of other nonhexagonal NGRs which clearly are not real molecules, but their “spatial evolution” would be expected to approach graphene. To this end, in Figure 7, we have summarized some representative results for nanographene/graphene models (in the order of increasing size) rectangular in their majority, of various sizes and geometries (including edge morphology).

One general characteristic emerging in Figure 7 is the CIRCO aromaticity pattern either in a free or “pure” form (1, 4, 5, 7) or in a “staggered or “frustrated” form (2, 3, 6, 9, 10, 11). A way to go from one form to the other by suitably manipulating the boundaries will be further discussed below, although a careful comparison of the structures in the figure could be highly suggestive about this. A second feature, which could have rather been expected, is the much higher aromaticity of the regions near the armchair edges (arranged top to bottom in the figure) in comparison to zigzag edges (arranged left to right). Both of these features will be further elaborated below.

Some of the specific characteristics of the structures in Figure 7 are summarized in Table 1. Structure 1 ($C_{54}H_{18}$) is a real molecule (serving as a model but not in the sense of the rectangular structures in the figure), the well-known circumcoronene (an *ortho*- and *peri*-fused polycyclic arene), which can be visualized as a complete circumference of rings around coronene. Its aromaticity pattern CIRCO (by definition) is similar to hexabenzocoronene (HEXCO) and satisfies both Clar’s rule (Clar’s formula) and the traditional Huckel $(4n+2)\pi$ electron rule. As will be illustrated below in section 3.3, these two fundamental rules are practically equivalent for NGRs and PAHs of hexagonal symmetry. The hexagonal (D_{6h}) symmetry is absolutely critical for such equivalence.

This becomes immediately clear when considering structure 2, $C_{54}H_{20}$, which has exactly the same number of carbon atoms as 1, and therefore the same number of π electrons (and about the same number of H atoms), but has rectangular D_{2h} symmetric geometry, which is characterized by three armchair rings and four zigzag rings in the perimeter (3×4). Its aromaticity pattern, in place of the one CIRCO in 1, consists of

two interpenetrating incomplete or “frustrated” CIRCO schemes, which are geometrically restricted horizontally by the small width (three rings) of the structure. In 4, in which four (4×2) more armchair (A) rings were added in the width (keeping the height (Z) the same), the interpenetrating double CIRCO scheme is completed, as can be seen in Figure 7a, whereas, in structure 3 in which two (2×2) zigzag rings were added (with the same number of armchair rings), the aromaticity pattern is “frustrated incomplete”. Structure 3 is peculiar in that its top and bottom layer is three rings wide as in 2 but the second row and the row before the last contain four rings; i.e., the second from the top and the second from the bottom rows contain more rings than the outer top and bottom rows, unlike in structures 2 and 4. Due to the D_{2h} symmetry, the half bottom part of the pattern should be the mirror image of the top, and there is a “horizontal” symmetry frustration of the interpenetrating incomplete CIRCO patterns. Structure 5 is a $4A \times 6Z$ structure in which the free and complete CIRCO pattern has developed. This structure was originally obtained from the $6A \times 8Z$ structure (9), which is a central reference structure in this work, by removing two peripheries of rings. This result should be better understood further below, where systematically we add or remove peripheral layers of rings. Structure 6 was obtained from 3 by adding one ring in the bottom layer (so as to have a total of four) and one more layer of four rings attached. This structure now has C_{2v} symmetry, since the top layer, in contrast to the rest, consists of three rings, and there is no any horizontal symmetry frustration, as in 3. As a result, the incomplete top CIRCO is repeated (slightly weaker) in the bottom. Structure 7 is the hexagonal Clar type PAH, $C_{114}H_{30}$, which we have examined before in Figure 4. This exemplifies the development of a multiple complete CIRCO pattern. On the other hand, the NICS(1) map in 8, consisting of two separated complete CIRCO patterns, can be considered as the vertical development of the incomplete CIRCO of 6. However, 8 should also be considered as “incomplete” or “frustrated”, not only because the peripheral “aromatic” rings near the zigzag edges are characterized by NICS(1) values of about 10.0 ppm (smaller than benzene) but mainly because the two CIRCO patterns are interrupted (touch) at the central region. Structure 9 is a $6A \times 8Z$ reference NGR with stoichiometry $C_{204}H_{40}$. As we can see in Figure 7b, its aromaticity pattern is just a simple but incomplete lateral

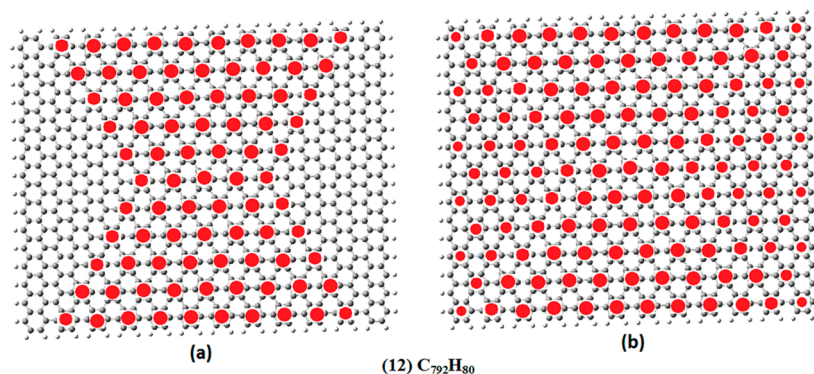


Figure 8. (a) Aromaticity pattern of the largest graphene model C₇₉₂H₈₀. (b) Extended aromaticity pattern.

expansion of the 4A × 8Z (8) double CIRCO pattern. Structure 10, 8A × 6Z, is a “conjugate” of 9, in the sense that the number of armchair bonded rings of one is equal to the number of zigzag bonded rings of the other. The aromaticity pattern of 10 is similar to that of 9 except for the middle horizontal region, due to geometrical (smaller width) restrictions. Finally, the aromaticity pattern of 11, which is a D_{2h} 8A × 8Z rectangular model, is just a “naturally” repeated and interconnected version of 8 which is a 4A × 8Z NGR.

Thus, it becomes clear that the NICS (aromaticity) patterns in Figure 7 are as follows:

- (a) complete pure CIRCOs in full agreement with Clar’s rule, either isolated (1, 5) or interconnected (4, 7)
- (b) incomplete (size restricted) CIRCOs which are consistent with Clar’s rule (2, 6)
- (c) complete touching pure CIRCOs which are not consistent with Clar’s rule (8, 11)
- (d) incomplete (symmetry restricted) CIRCOs which are not consistent (touching “aromatic” rings) with Clar’s rule (3, 9)

As was illustrated above (e.g., consider structures 2, 3, and 4), one can transform from one category to the other by simple geometrical transformations, keeping the same symmetry (D_{2h}), or even the same edge structure. This will be further discussed below in subsection 3.3.

It becomes clear that in all cases examined here the CIRCO pattern in all its forms (incomplete, frustrated, or touching) is dominant in the structures of Figure 7, although the rectangular arrangements in the NICS patterns with touching CIRCOs (as in structures 3, 8, 9, and 11) could be seen as the rectangular (D_{2h}) analogues of CO patterns. In this respect, structures 3, 8, 9, and 11, classified in the categories c and d above, could be considered as mixed CO and CIRCO patterns. In that case, it seems that the pure CO and CIRCO patterns do not mix only in hexagonal D_{6h} geometries. This will be further considered in section 3.3. The rectangular NGRs (4 and 5) belong to the category (a) of pure CIRCO or Clar type aromaticity patterns. The incomplete CIRCO scheme is due to size, in connection to symmetry, restrictions or else to the morphology of the boundaries. This is because in finite size systems, as the ones examined so far, the presence of particular edge configurations could disrupt the distribution of all π electrons (of the boundary carbons) into Clar sextets. In general, the edges of PAHs and NGRs can impose a Clar formula consisting of a mixture of localized double bonds and Clar sextets. This is true not only for the geometry optimized PAHs (also nanoribbons and nanotubes) but also for the rectangular NGR models for

which the bond length was kept constant and equal to 1.42 Å. In this case, geometry optimization does not usually affect the overall NICS(1) pattern, although it generally reduces the NICS(1) values toward the zigzag edges. With or without optimization, the armchair edges are among the most aromatic regions (regions with larger absolute values of NICS(1)). For infinite graphene or for large enough NGRs, the boundary effects (and restrictions) would be gradually diminishing, revealing the real aromaticity pattern of pristine graphene, which on the basis of the preceding discussion would be expected to be of the CIRCO Clar type. In Figure 8, we show the NICS(1) aromaticity pattern of a very large 12A × 16Z NGR with stoichiometry C₇₉₂H₈₀, consisting of 872 atoms and 4832 active electrons (all electrons are included in the DFT calculation).

In Figure 8a, the aromaticity pattern is shown for high (~ -16 ppm) and medium (~ -11 ppm) NICS(1) values, shown with larger and medium size aromatic circles, respectively. As we can see, this pattern, which is fully CIRCO type, evolves from the central region (top to bottom) with very aromatic armchair edges toward the (left–right) zigzag edges. This is verified in Figure 8b in which aromatic rings with NICS(1) values between -11.2 and -8.5 ppm (up to 75% of benzene) are included in the scheme (with smaller and much smaller circles). Thus, assuming that Figure 8b represents a subsection of the infinite graphene lattice, we can see that the primary aromaticity pattern of graphene is a full CIRCO scheme (represented by Figure 8b in which we can ignore the boundaries and the corresponding differences in the size of the circles). This pattern forms a (√3 × √3)R30° superlattice in full agreement with Clar’s theory.^{7,8,10,20} In this scheme, each aromatic ring (indicated with a full circle) is surrounded by six nonaromatic (“empty”) rings. However, since graphene is characterized by a constant bond length of 1.42 Å and a uniform π electron distribution, its actual aromaticity pattern should be a superposition of primary patterns in which full and empty rings are interchanged. This will be further elaborated in section 3.3 in which the bond length of 1.42 Å will also be rationalized. Looking carefully at the central portion of Figure 8b (to avoid edge effects), we can see that the empty rings form a coronene CO type pattern. Thus, the actual aromaticity pattern of infinite (pristine) graphene should be a superposition of CIRCO and CO patterns. Clearly, this is a new concept of delocalization well beyond the traditional notion of local and global aromaticity involving a coordinated collective effect. We arrive at the same conclusion in a more straightforward way in section 3.3. However, this is not totally new. As we have mentioned earlier,

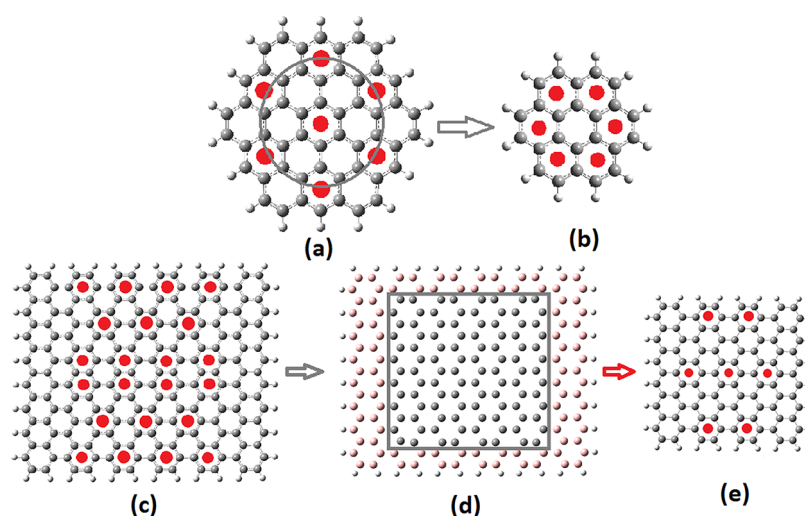


Figure 9. Schematic diagram showing the structural and aromatic changes in systems with (a, c) and without (b, e) an outer perimeter of rings (outside the gray frames), circumcoronene and coronene on the top, and NGR structures (9) and (5) on the bottom. In part d, the intermediate step from (c) to (d) is illustrated schematically, without the bonds for clarity.

Zubarev et al.¹⁴ have illustrated using a completely different approach based on cellular automata (CA) that bonding in graphene is a collective effect beyond the notion of local and global aromaticity. It is interesting to observe that at the level of optimized PBE0/6-31g* geometries the bond length of the central ring of circumcoronene is 1.415 Å and the one in the next layer 1.425 Å with a clear average of 1.42 Å which is the bond length of graphene. The corresponding values for coronene (at the same level of theory) are 1.423 and 1.416 Å, respectively, with an average value of 1.419(5) Å. As will be further explained below, this is in full agreement with the periodic changes in the aromaticity patterns of nanographenes as a new periphery of rings is added or removed. Therefore, unlike infinite graphene, for finite graphene flakes, or, more generally, every time the periodicity is interrupted (for instance, at the boundaries), the “uniform” aromaticity pattern would get uncoupled and be “tuned” to the boundary conditions. This should be very important for nanographene flakes, graphene ribbons and nanotubes, and any other finite or semifinite graphene model.

3.2. From Graphene to NGR Nanoribbons and Nanotubes. On the basis of the above discussion, it would be expected that, for a finite (in one or two dimensions) graphene, the aromaticity pattern would uncouple and get tuned to the particular size and boundary. For a given size and edge structure, the aromaticity pattern would be some analogue of one of the patterns in Figure 7. However, by properly manipulating the boundary (and the size) of the NGR, we could get sooner or later the primary CIRCO aromaticity pattern of graphene. A good example of this was given above in the comparison of structures 2, 3, and 4. Thus, addition or removal of one or more peripheral layers of rings would change the aromaticity pattern. This should also be true for PAHs, seen as finite graphene models, as in NGRs. In Figure 9, we show schematically this type of relation between coronene and circumcoronene on the top and between structures 5 and 9 on the bottom. To study this effect more systematically, we consider in Figure 10 systematic successive variations by one periphery in the $8A \times 8Z$ structure (11). For these results to be fully meaningful, the (finite) structures are geometrically

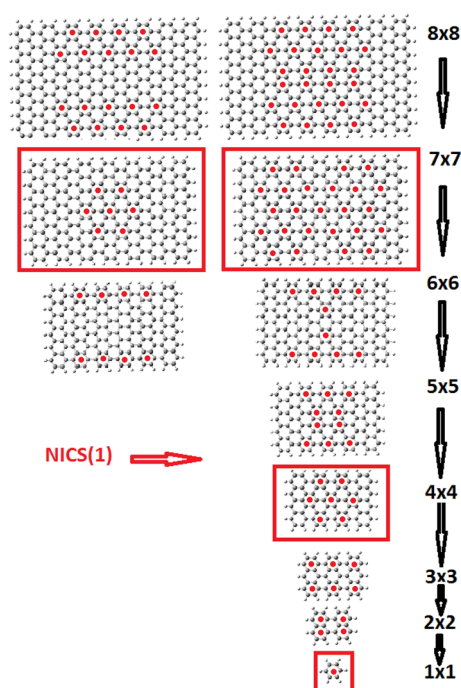


Figure 10. Variation of the aromaticity pattern in terms of periphery. For the three largest structures (8×8 , 7×7 , and 6×6), the NICS(1) pattern on the left includes only the major NICS(1) value, as listed in Table 2 (NICS H) $\pm 5\%$.

optimized and their main characteristics before and after geometry optimization are listed in Table 2.

In Table 2, we show at the same time results regarding the variation of the electronic and cohesive characteristics with geometry optimization as well as with system size. As we can see in Figure 10, every 3 perimeters variation, we have a periodical variation of the aromaticity pattern. The periodic cycle includes

- (a) complete or incomplete (due to size restrictions) touching CIRCO patterns, not consistent with Clar's rule (as 8×8 , 5×5)

Table 2. NICS(1) Values: Higher (NICS H) and Lower (NICS L) before (Top of the Row) and after (Bottom of the Row) Optimization; HOMO–LUMO Gaps (H–L Gap) before (Top of the Row) and after (Bottom of the Row) Optimization; Binding Energies (E_{bnd}), Average (b_{av}) and Longer/Shorter (b L/S) Bond Lengths of the Optimized Structures^a

Struc AxZ	NICS H ppm	NICS L ppm	H-L (eV)	E_{bnd} (eV)	b_{av} Å	b L/S Å
8x8	-14.1	-12.3	0.25			
8x8-Opt	-14.4	-12.4	0.36	8.08	1.417(3)	1.442
7x7	-14.7	-11.1 (-10.0)	0.13			1.368
7x7-Opt	-15.9	-12.4 (-10.4)	0.31	8.13	1.416(9)	1.451
6x6	-12.2	-10.6 (-10.2)	0.15			1.367
6x6-Opt	-12.4	-10.3 (-9.8)	0.15	8.20	1.416(6)	1.455
5x5	-12.4	-11.2 (-10.5)	0.19			1.371
5x5-Opt	-12.8	-11.5 (-10.6)	0.19	8.29	1.416	1.455
4x4	-14.0	-12.7 (-11.2)	0.30			1.373
4x4-Opt	-13.8	-12.6 (-10.6)	0.32	8.42	1.415	1.458
3x3	(-8.3)	(-8.3)	0.97			1.371
3x3-Opt	(-8.4)	(-8.6)	1.24	8.63	1.413	1.471
2x2	(-9.0)	(-9.0)	2.88			1.372
2x2-Opt	(-9.7)	(-9.7)	3.35	9.03	1.409	-----
1x1	-11.4	-11.4	7.25	10.1	1.393	-----

^aThe latter (struc.) are described by the number of armchair (A) and zigzag (Z) rings in their periphery (A × Z). Shaded areas show results at the non-optimized geometry.

- (b) complete CIRCO pattern(s), fully consistent with Clar’s rule (such as 7×7 , 4×4); we call these species aromatic
(c) not recognizable CIRCO patterns (as 6×6 , 3×3); we can call these structures Kekulé type in analogy to the term used for nanotubes¹³

On the basis of this periodical scheme, we can predict that 9×9 would be a Kekulé type nonaromatic, whereas 10×10 would be a full CIRCO aromatic structure. From Table 2, it can be seen that the periodicity in the aromaticity pattern, which is also evident in the values of NICS(1) H, is not accompanied by a periodicity in the binding energy (which varies monotonically with size) or by a periodicity in the H–L gap, perhaps due to quantum confinement. However, the aromatic 7×7 structure has a significantly larger gap from the nearby 6×6 (after optimization) which is smaller and would be expected with a larger gap due to quantum confinement. Similarly, the aromatic 4×4 NGR has a significantly larger gap from the 5×5 but not

from 3×3 , which however is a limited case and is expected to be dominated by quantum confinement. Furthermore, the average bond length of the optimized structures remains practically the same (at least for the five largest NGRs), close to 1.420 Å, which is the nonoptimized value. This value drops gradually to 1.41 Å and eventually to 1.39(3) Å for benzene (always at the level of PBE0/6-31G*). The maximum bond length, occurring around the zigzag edges, fluctuates between 1.44 and 1.46 Å, whereas the minimum bond length (around the armchair edges) is almost constant around 1.37 Å. In Figure 10 (and Figure 8b), in several cases, in order to bring up the full CIRCO (or HEXCO) pattern, we have included in the diagram NICS(1) values smaller in magnitude from the one of benzene (down to 75% |−11.4 ppm|, at most). Usually this involves rings toward the zigzag edges. For example, similarly to Figure 8b, for the aromaticity pattern of 7×7 , we have included in the NICS(1) diagram the two pairs of “aromatic” rings farthest toward the zigzag edges, which are characterized by NICS(1) = −10 ppm (see also Table 2).

It becomes clear that the periodicities of the aromaticity patterns of finite NGRs (and by extension the periodicities in nanoribbons and nanotubes) can be understood from the primary aromaticity pattern of graphene in Figure 8b. From the periodicity of this scheme (assuming that Figure 8b represents only a section of the infinite lattice), it becomes clear that, if we start from the central ring and draw successive circles containing the centers of neighboring rings in terms of distance, every three neighbor circles (i.e., every third shell of distant neighbors of the $(\sqrt{3} \times \sqrt{3})R30^\circ$ superlattice), we would encounter again (we will regenerate) the full (multiple) CIRCO motive. Therefore, every three additional peripheries (shells of ring-neighbors), we should have the same periodicity scheme within the given boundaries. Such a periodicity cycle is related to the overall rectangular symmetry (D_{2h} in Figure 10), as will be verified in the next section.

3.3. From Hexagonal PAHs to Graphene. Obviously, the route shown by the vertical arrows in Figure 10 can be reversed to lead from benzene to graphene eventually. However, the rectangular D_{2h} NGR models are rather arbitrary or even fictitious. Moreover, to build more and more surface layers, we have two independent degrees of freedom (width and height), although we have avoided this problem in Figure 10 by considering NGRs with an equal number of armchair (A) and

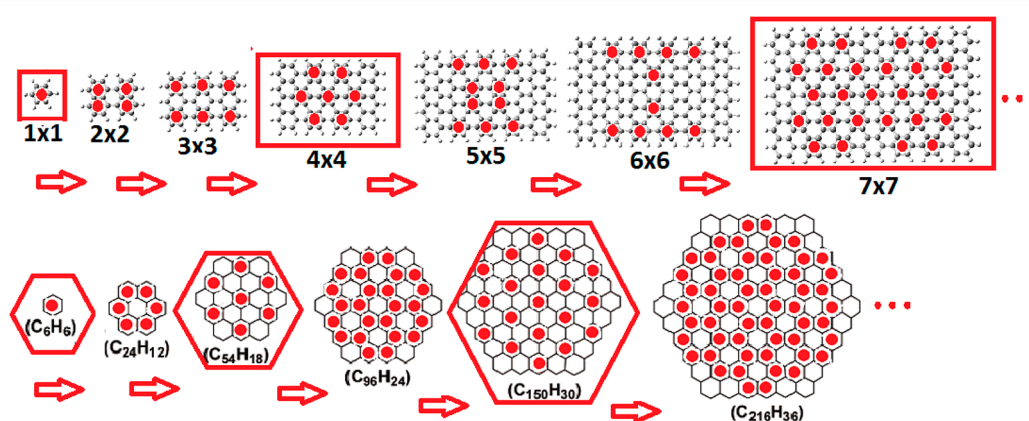


Figure 11. Variation of the aromaticity pattern in terms of circumference addition(s), for D_{2h} (top) and D_{6h} (bottom) symmetric samples. The upper portion of the figure with rectangular nanographenes is similar to Figure 10. The lower portion is similar to Figure 3 of Moran et al.⁴ for their PAH structures 1–6.

zigzag (Z) rings. A better and more realistic way would be to consider a sequence of real hexagonal PAHs with first member benzene followed by coronene and circumcoronene (as in Figure 9), etc. This has been done in Figure 11. As we can see in the figure, for the D_{6h} symmetric structures, each additional periphery changes the aromaticity pattern from coronene (CO) type to circumcoronene (CIRCO) and vice versa. Thus, the periodicity scheme involves only two members.

As we can verify in Figure 11, for the coronene type of aromaticity pattern, the number of carbon atoms N is a multiple of 4, i.e., $N = 4n$, whereas for CIRCOs we have $N = 4n + 2$, which is equivalent to the traditional Huckel $(4n+2)\pi$ electron rule, since N is also the number of π electrons, with benzene clearly falling into the CIRCO type with $n = 1$. The two patterns alternate as we add more and more layers of rings, and so does the Huckel criterion. If k is the number of layers around benzene (which corresponds to $k = 0$), the number of carbon atoms (and, therefore, of π electrons) in the sequence of PAHs in Figure 11 is given by²¹ $N = 6(k + 1)^2$. From this, it can be easily seen that successive structures in the figure, which correspond to successive layer addition (successive k values), would be characterized by alternative CIRCO (k even) and CO (k odd) aromaticity patterns, corresponding to $4n+2$ and $4n$ π electrons, respectively. It is clear that this rule applies not only to the structures of Figure 11b, obtained by successive peripheral additions of rings, but to all hexagonal structures (or at least to all hexagonal structures examined here). Hexabenzocoronene ($C_{42}H_{18}$), for example, fulfills the $4n+2$ criterion and is characterized (as we have seen in Figure 2) by a HEXCO/CIRCO aromaticity pattern. Thus, the CIRCO pattern corresponds to the well-known Huckel rule for aromatic molecules, whereas the CO pattern could be loosely interpreted as “Huckel anti-aromatic”. However, as we have seen in section 2.1 and exemplified in Figure 1, coronene itself, which is the prototype and the smaller member of the CO patterned PAHs, is believed to be superaromatic, which is explained in Clar’s theory by invoking “migrating sextets”,⁴ as shown in Figure 1a. In a different approach, Popov and Boldyrev²² using the adaptive natural density partitioning method concluded that coronene has two globally delocalized concentric π systems, whereas circumcoronene does not have globally delocalized π systems; instead, it has seven local Clar sextets represented by a single Clar structure (CIRCO), as in 1 in Figure 7. The exact type of aromaticity of coronene and circumcoronene is a subject beyond the target and the spirit of the present work. Similarly, more information on the application of these ideas to other finite size (width) graphene systems, such as nanoribbons and nanotubes,^{10–13,23,24} as well as the influence of edge effects²⁵ on their aromaticity patterns can be found in the literature.^{10–13,23–25} Thus, independently of the Huckel $(4n+2)\pi$ electron rule (which is strictly valid for monocyclic systems), we are led to accept that both types of patterns (CO and CIRCO) are aromatic, perhaps at a different level of delocalization (“global” or “local”, etc.).

The route toward graphene is by now rather clear. Every time a new hexagonal periphery is added, the CIRCO and CO patterns are successively interchanged, or equivalently “Huckel aromatic” and “Huckel anti-aromatic” PAHs alternate. In the limit of infinite graphene, if this trend continues indefinitely, we would expect that the two results (from the k th and $k+1$ th “peripheries”) should be equivalent. Thus, although the primary aromaticity pattern of graphene would be the fully aromatic (in the sense of Huckel’s rule) CIRCO type, the “complementary”

CO pattern (which, as we can see in the central portion of Figure 8b, is formed by the empty rings of the “infinite” lattice) would also be present in the actual aromaticity pattern of infinite graphene. In other words, the actual pattern of graphene would be a superposition of the two CIRCO and CO patterns. As a result, the bond length of graphene, 1.42 Å, should be the average of the two. Indeed, as was mentioned before, at the level of optimized PBE0/6-31g* geometries, the bond length of the central ring of circumcoronene is 1.415 Å and the one in the next layer is 1.425 Å with a clear average of 1.42 Å. The corresponding values for coronene (at the same level of theory) are 1.423 and 1.416 Å, respectively, with an average value of 1.419(5) Å. Alternatively, the average of the central ring bond lengths of circumcoronene and coronene is again 1.419(5) Å. All of this is indicative of the essential correctness of the resonance idea presented here. Thus, our results are in full accord with Pauling’s resonance idea, and the collective delocalization of Zubarev et al., which leads to a “self-organized criticality” (SOC). Zubarev et al.¹⁴ have demonstrated that a local perturbation (such as chemisorption of a H atom in an “internal” C atom) of the π electron system (consisting of a rectangular NGR with stoichiometry $C_{284}H_{46}$) generates re-equilibration of C–C distances (in clusters of various sizes), with the distribution of domain sizes obeying a power law, suggesting a scale-invariant response, and therefore a form of SOC. This outlook acquires special significance in view of recent reports by Wang et al.,²⁶ who demonstrated that electrons in graphene behave like a critical system in the presence of Coulomb interactions. The present approach, without the sophistication (and the complexity) of other advanced methods, such as those of Zubarev et al.¹⁴ or Wang et al.,²⁶ using the DFT framework, which includes electron correlation at the PBE0¹⁸ level, and widespread and well-tested tools (such as NICS), leads in a simple and transparent way to essentially the same picture, which is clearly one step beyond the usual concepts of local or global electron delocalization. Moreover, our present methodology gives much more useful, new, and reproducible information for finite-size systems as well. In full agreement with Clar’s theory, the present results illustrate that for finite (or nonfully periodic) samples the primary CIRCO (Clar’s) pattern will be the dominant pattern present, should the boundary conditions allow it. In this sense, our results make it clear that the periodic CIRCO scheme is the underlying primary reason for the observed aromatic periodicities in NGRs and PAHs (revealed here), as well as in nanoribbons and nanotubes.^{11–13,20,24,25}

4. CONCLUSIONS

Using the present real space nucleus independent chemical shifts (NICS)-based scheme (NICS maps), which is widespread and well tested (certainly not free of criticism), we have treated graphene and the various types of nanographenes (NGRs) and PAHs on an equal footing, as large size molecules whose dimensions and geometries were judiciously selected to bring up and carefully test the important electronic and aromatic features, and especially to interrelate the “molecular” (finite) and “crystalline” (infinite) features and regularities. We have made an effort to keep the whole process as simple and transparent as possible, avoiding unnecessary and/or obscure complications and possible fruitless disputes, in view of the subtle and/or controversial character of the subject.^{1–5,9,16} This is the main reason we have avoided other promising more recent theoretical techniques such as the “superaromatic

stabilization energy” method, applied by Sakamoto et al.,¹⁹ or the six-center index (SCI) used by Martin-Martinez,²⁵ for several PAHs of various sizes and finite-length nanoribbons. Nevertheless, for all common PAHs we have examined here, we have obtained identical results for the aromaticity patterns, with apparently less computational effort. Using the simplest and more well-established methodology,³ we have discovered a new important periodical principle in the aromatic (and electronic) properties of nanographene(s) and PAHs in terms of circumferential growth from which not only the observed periodicities in the aromaticity of nanotubes and nanoribbons can be deduced but also the primary and the actual resonance aromaticity pattern of (infinite) graphene can be inferred, interrelating with finite size “graphene fragments” and rationalized in terms of Clar’s empirical scheme.^{7,8} In summary, the following has been illustrated:

- There is a “universal” primary aromaticity pattern of graphene made up of aromatic (full) rings forming periodic CIRCO subunits, which is surrounded by empty (nonaromatic) rings, arranged in a complementary coronene (CO) type of arrangement. These two fundamental CIRCO and CO patterns are successively interchanged in finite hexagonal (D_{6h} symmetric) PAHs of the form shown in Figure 11, every time a new circumference of rings is added in (or removed from) their periphery.
- It is illustrated that D_{6h} symmetric PAHs in which the number of carbon atoms N is of the form $N = 4n + 2$ (with n integer) are characterized by the CIRCO pattern, whereas those with $N = 4n$ are of the CO type. This is equivalent to the traditional Huckel $(4n+2)\pi$ electron rule.
- Furthermore, this interchange of CIRCO and CO patterns in the limit of infinite graphene should naturally lead to the anticipated linear combination of CIRCO and CO patterns, since the results from the k th and $k+1$ th “peripheries” should be equivalent.
- This is in full accord with the conclusions of Zubarev et al.,¹⁴ who demonstrated that delocalization in graphene is an intrinsically collective effect, beyond the concept of local and global aromaticity.
- Thus, graphene should fit to the description of a “resonance structure” along the lines of Pauling’s initial suggestion.¹⁵
- When the periodicity is interrupted (e.g., at the boundaries), the aromaticity pattern is predicted to get uncoupled and “tuned” to the boundary conditions.
- For rectangular (D_{2h} symmetric) nanoflakes as in Figure 10, the periodicity cycle involves three members (we have the same pattern every three additional peripheries (shells of ring-neighbors). This is naturally extended to nanoribbons and nanotubes.
- For finite or semifinite graphene structures which include both armchair and zigzag edges, the armchair edges and the region surrounding them are substantially “more aromatic”, compared to zigzag edges (see, for instance, Figure 8).
- The present results should be very important for the rationalization and functionalization of the electronic and aromatic properties of graphene and of the various forms of nanographenes, PAHs, GNRs, and nanotubes.

AUTHOR INFORMATION

Corresponding Author

*E-mail: zdetsis@upatras.gr.

Notes

The authors declare no competing financial interest.

ACKNOWLEDGMENTS

This work was supported by the EU- ERC project PHOTO-META No. 320081.

REFERENCES

- (1) Schleyer, P.v.R. Introduction: Aromaticity. *Chem. Rev.* **2001**, *101*, 1115–1118.
- (2) Schleyer, P.v.R. Introduction: Delocalization—Pi and Sigma. *Chem. Rev.* **2005**, *105*, 3433–3435.
- (3) Sola, M.; Feixas, F.; Jimenez-Halla, J. O. C.; Matito, E.; Poater, J. A critical assessment of the performance of magnetic and electronic indices of aromaticity. *Symmetry* **2010**, *2*, 1156–1179.
- (4) Moran, D.; Stahl, F.; Bettinger, H. F.; Schaefer, H. F., III; Schleyer, P. v. R. Towards graphite: Magnetic properties of large polybenzenoid hydrocarbons. *J. Am. Chem. Soc.* **2003**, *125*, 6746–6752.
- (5) Popov, I. A.; Bozhenko, K. V.; Boldyrev, A. I. Is Graphene Aromatic? *Nano Res.* **2012**, *5*, 117–123.
- (6) Gutman, I.; Tomovic, Z.; Mullen, K.; Rabe, J. P. On the distribution of p-electrons in large polycyclic aromatic hydrocarbons. *Chem. Phys. Lett.* **2004**, *397*, 412–416.
- (7) Clar, E. *The aromatic sextet*; Wiley: New York, 1972.
- (8) Sola, M. Forty years of Clar’s aromatic π -sextet rule. *Front. Chem.* **2013**, *1*, 22.
- (9) Schleyer, P.v.R.; Maerker, C.; Dransfeld, A.; Jiao, H.; van Eikema Hommes, N. J. R. Nucleus independent chemical shifts: A simple and efficient aromaticity probe. *J. Am. Chem. Soc.* **1996**, *118*, 6317–6318.
- (10) Wassmann, T.; Seitsonen, A. P.; Saitta, A. M.; Lazzeri, M.; Mauri, F. Clar’s theory, π -electron distribution, and geometry of graphene nanoribbons. *J. Am. Chem. Soc.* **2010**, *132*, 3440–3451.
- (11) Martin-Martinez, F. J.; Fias, S.; Van Lier, G.; De Proft, F.; Geerlings, P. Tuning aromaticity patterns and electronic properties of armchair graphene nanoribbons with chemical edge functionalisation. *Phys. Chem. Chem. Phys.* **2013**, *15*, 12637–12647.
- (12) Martin-Martinez, F. J.; Fias, S.; Hajgato, B.; Van Lier, G.; De Proft, F.; Geerlings, P. Inducing aromaticity patterns and tuning the electronic transport of zigzag graphene nanoribbons via edge design. *J. Phys. Chem. C* **2013**, *117*, 26371–26384.
- (13) Matsuo, Y.; Tahara, K.; Nakamura, E. Theoretical studies on structures and aromaticity of finite-length armchair carbon nanotubes. *Org. Lett.* **2003**, *5*, 3181–3184.
- (14) Zubarev, D. Y.; Frenklach, M.; Lester, W. A., Jr. From aromaticity to self-organized criticality in graphene. *Phys. Chem. Chem. Phys.* **2012**, *14*, 12075–12078.
- (15) Pauling, L. The nature of the chemical bond and the structure of molecules and crystals: An introduction to modern structural chemistry; Cornell University Press: Ithaca, NY, 1960.
- (16) Tsepis, A. C.; Depastas, I. G.; Tsepis, C. A. Diagnosis of the σ -, π - and $(\sigma+\pi)$ -aromaticity by the shape of the NICSzz-scan curves and symmetry-based selection Rules. *Symmetry* **2010**, *2*, 284–319.
- (17) Frisch, M. J.; Trucks, G. W.; Schlegel, H. B.; Scuseria, G. E.; et al. *Gaussian 09*, revision C.01; Gaussian, Inc.: Wallingford, CT, 2009.
- (18) Adamo, C.; Barone, V. Toward reliable density functional methods without adjustable parameters: The PBE0 model. *J. Chem. Phys.* **1999**, *110*, 6158–616969.
- (19) Sakamoto, K.; Nishina, N.; Enoki, T.; Aihara, J. Aromatic character of nanographene model compounds. *J. Phys. Chem. A* **2014**, *118*, 3014–3025.
- (20) Wu, D.; Gao, X.; Zhou, Z.; Chen, Z. Understanding aromaticity of graphene and graphene nanoribbons by the clar sextet rule.

Graphene Chemistry: Theoretical Perspectives; John Wiley & Sons: 2013, 29–49; DOI: 10.1002/9781118691281.

(21) Stein, S. E.; Brown, R. L. π -Electron Properties of large condensed polyaromatic hydrocarbons. *J. Am. Chem. Soc.* **1987**, *109*, 3721–3729.

(22) Popov, I. A.; Boldyrev, A. I. Chemical bonding in coronene, isocoronene, and circumcoronene. *Eur. J. Org. Chem.* **2012**, *2012*, 3485–3491.

(23) Zhang, X.; Xin, J.; Ding, F. The edges of graphene. *Nanoscale* **2013**, *5*, 2556–69.

(24) Wassmann, T.; Seitsonen, A. P.; Saitta, A. M.; Lazzeri, M.; Mauri, F. Structure, stability, edge states, and aromaticity of graphene ribbons. *Phys. Rev. Lett.* **2008**, *101*, 096402.

(25) Martin-Martinez, F. J.; Fias, S.; Van Lier, G.; De Proft, F.; Geerlings, P. Electronic structure and aromaticity of graphene nanoribbons. *Chem. - Eur. J.* **2012**, *18*, 6183–6194.

(26) Wang, J.; Fertig, H. A.; Murthy, G. Critical behavior in graphene with Coulomb interactions. *Phys. Rev. Lett.* **2010**, *104*, 186401.